IEEE Robotics and Automation Letters (RAL) paper presented at the
2020 IEEE/RSJ International Conference on Intelligent Robots and Systems (IROS)
October 25-29, 2020, Las Vegas, NV, USA (Virtual)

Optimization-Based Investigation of Bioinspired Variable Gearing of the Distributed Actuation Mechanism to Maximize Velocity and Force

Jong Ho Kim, and In Gwun Jang, *Member, IEEE*

Abstract—**Transmission between high speed and high force motions is a classic, but challenging problem for most engineering disciplines as well as robotics. This study optimizes the performances (i.e., both velocity and force) of the distributed actuation mechanism (DAM) based on the novel concept of continuously variable gearing, which is inspired by muscle movement. To quantify continuously variable gearing in the DAM, the structural gear ratio (defined as joint speed/motor speed) is mathematically derived in terms of the slider position and the joint angle. Then, for a DAM-based three-revolute joint manipulator, a multi-objective optimization problem is formulated to determine the maximum end-effector velocity according to varying payloads. An optimization framework consisting of the analysis and optimization modules is constructed to verify the proposed concept with a comparison of an equivalent joint actuation mechanism (JAM)-based three-revolute joint manipulator. The numerical results demonstrate that the bioinspired variable gearing of the DAM allows for a significant enhancement of end-effector velocity and force, depending on a given task.**

I. Introduction

In robotics, joint actuation is generally performed by electric motors. Because typical electric motors have a small torque and high speed, the use of a transmission with a reduction gear ratio is mandatory. Therefore, the performance of the robot, which is typically aimed to achieve either high speed or high force, is affected depending on the gear ratio selected. A simple and effective solution to this classic engineering contradiction between speed and force is to physically adjust the optimal gear ratio for a given task.

The most common example of changing gear ratios for transmission is the vehicle powertrain system. A typical vehicle equipped with multiple gears operates at a certain fixed gear ratio that allow it to run efficiently in each speed range and shifts a gear ratio when necessary. On the other hand, a continuously variable transmission (CVT) provides an incessant changes of gear ratios, thereby increasing the fuel economy and dynamic performance of a vehicle by better balancing the engine operating conditions under time-varying driving circumstances [1].

In the field of robotics, research on variable gearing has been recently conducted. A dual mode twisting mechanism has been proposed to achieve either high speed or high force motion by discretely shifting the radius of the twisted string [2] [3]. To achieve high-speed motion and large grasping force, a grasping-force-magnification mechanism was similarly proposed in [4]. Actively variable transmission based on crank-slider kinematics was proposed for several situations such as walking, and stair ascent and descent [5].

There has also been a study on the CVT mechanism for continuously variable gearing. A method of continuously shifting gears has been proposed by replacing the teeth of the strain wave gears with soft frictional contact [6]. In [7], the gear ratio continuously changes by adjusting the effective pulley radius. As a continuously variable gearing system, a parallel-link manipulator was also proposed with several linear shaft motors in [8]. In [9], the rubber wheel, which spools the wire, continuously reduces the moment arm due to the passively decreased wheel radius under the increasing external load, thereby providing continuously variable gear ratio changes. However, in the aforementioned studies, it was not possible to actively control the gear ratio changes, but only passively by external force.

Meanwhile, variable gearing systems can be found in nature, with pennate muscles being an example. Pennate muscles are known to generate a large force, because it has muscle fibers in an oblique direction to the line of the external force [10]. As the muscle contracts, the fibers rotate more obliquely to the line of action, the angle of which is called the pennation angle. In [11], the ratio of muscle speed to fiber speed was defined as the architectural gear ratio, and it was found that this value varies with the load exerted on the muscle. It should be noted that a change in the pennation angle for muscle movement lead to a change in gear ratio. Then, this working principle of a pennate muscle was applied to a McKibben actuator array, and it was demonstrated that the architectural gear ratio changes according to load [12].

As a widely used engineering scheme, gradient-based optimization is a type of mathematical programming that can systematically and efficiently minimize or maximize the objective function (e.g., minimization of the assistive force by the robot and zero-moment-point error [13] and joint torque [14], or maximization of electrical energy for the energy harvester [15]) while satisfying the constraint functions (e.g., self-collision and singular configuration [16], physical

This research was supported by a grant (17TLRP-C135446-01, Development of Hybrid Electric Vehicle Conversion Kit for Diesel Delivery Trucks and its Commercialization for Parcel Services) from the Transportation & Logistics Research Program (TLRP), funded by the Ministry of Land, Infrastructure and Transport of the Korean government.

J. H. Kim and I. G. Jang are with the Cho Chun Shik Graduate School of Green Transportation, Korea Advanced Institute of Science and Technology (KAIST), Daejeon 34051, Korea. (e-mail: jonghokim@kaist.ac.kr, igjang@kaist.edu)

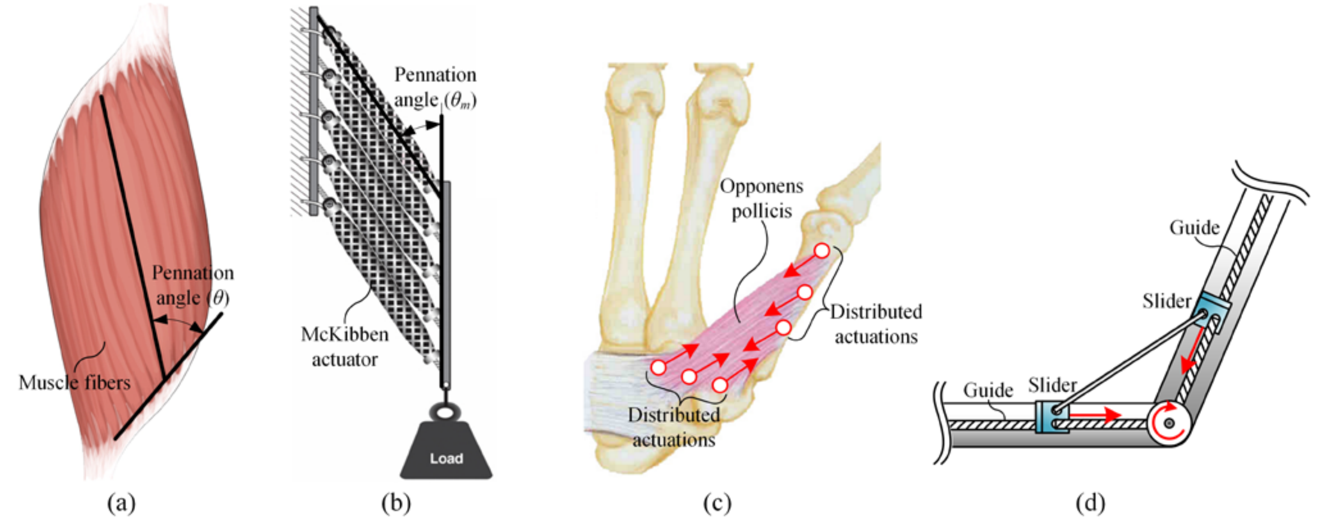

Fig. 1. Bioinspired variable gearing systems: (a) Pennate muscle [11], (b) Pneumatic actuator array [12], (c) Spatially distributed actuation of a finger [21], (d) Distributed actuation mechanism [13].

constraints of the sensor configuration [17]). Regarding gear ratio changes, the linear-to-rotary transmission ratio of the four-bar linkage mechanism was optimized [18]. To maximize the gripping force, the force transmission ratio was also maximized using genetic algorithm [19].

As another example of bio-inspired actuation mechanism, the distributed actuation mechanism (DAM) relocates the redundant actuation point of a slider to improve the fingertip force [20]. The DAM can adjust the joint torque simply by changing the position of the slider without changing a posture. This paper proposes the concept of the DAM-based bioinspired variable gearing and verifies it with the three-revolute joint manipulator. The structural gear ratio (SGR) of the DAM is defined and then is derived in terms of the slider position and the joint angle. Then, gradient-based optimization is conducted to determine the maximum velocity and force of the DAM-based three-revolute joint (DAM-3R) manipulator. For comparison, a joint actuation mechanism (JAM)-based three-revolute joint (JAM-3R) manipulator is investigated with the power-equivalent motors and the same geometric specification.

This paper is organized as follows. In Section II, the concept of bioinspired variable gearing in the DAM is explained. Then, the SGR is defined and mathematically expressed, based on the leadscrew actuation. Section III describes the simulation-based optimization that can determine the maximum performance of the DAM-3R manipulator. Then, the effects of the SGR are analyzed with a comparison of an equivalent JAM-3R manipulator. The conclusion follows in Section IV.

TABLE I Design Parameters of the DAM

		Lower Bound	*Upper Bound*
Design variables (to be determined)	θ **[°]**	20	90
	s **[mm]**	37.0	77.0
Design constants (fixed)	c **[mm]**	80	
	L **[mm]**	0.7	
	h **[mm]**	15.5	
	F_{max} **[N]**	55.79	

II. Bioinspired Variable Gearing of The DAM

A. Concept of the DAM-based Bioinspired Variable Gearing

Pennate muscles move with varying gear ratios by changing the pennation angle (θ in Fig. 1(a)), depending on the external load [11]. Based on this observation, a biomimetic pneumatic actuator array was proposed in [12]. Considering the above action of pennate muscles, the pneumatic actuator array can change the pennation angle (θ_m in Fig. 1(b)), which leads to a change in the gear ratio (Fig. 1(b)). Similarly, as shown in Fig. 1(c), the fundamental movement of human fingers, such as stretching or expanding, can be accomplished through contraction and relaxation of the flexor digitorum profundus, flexor digitorum superficialis, and extender digitorum [21]. Concurrently, sophisticated and dexterous movements can be achieved by the spatially dispersed actuation of opponens pollicis over the finger rather than by the lumped actuation. In [20], the spatially distributed actuation of opponens pollicis was implemented in the DAM by controlling a slider that moves along a link (Fig. 1 (d)). Ultimately, both systems control the force vector for variable gearing. However, it should be noted that the pneumatic actuator array change the direction of force to adjust the architectural gear ratio [12], whereas the DAM changes the point of application of the force [20]. This study will quantitatively investigate the DAM from the viewpoint of

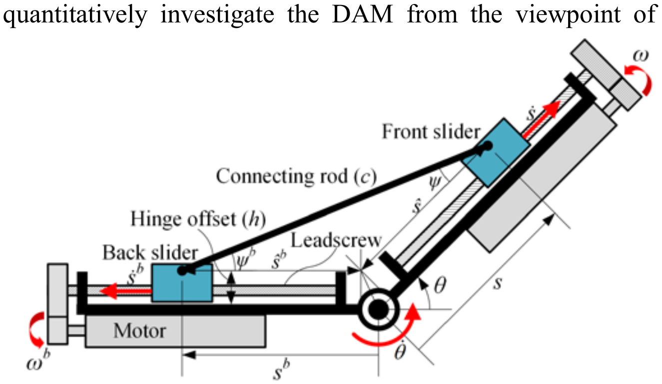

Fig. 2. Distributed actuation mechanism for a single joint using leadscrew.

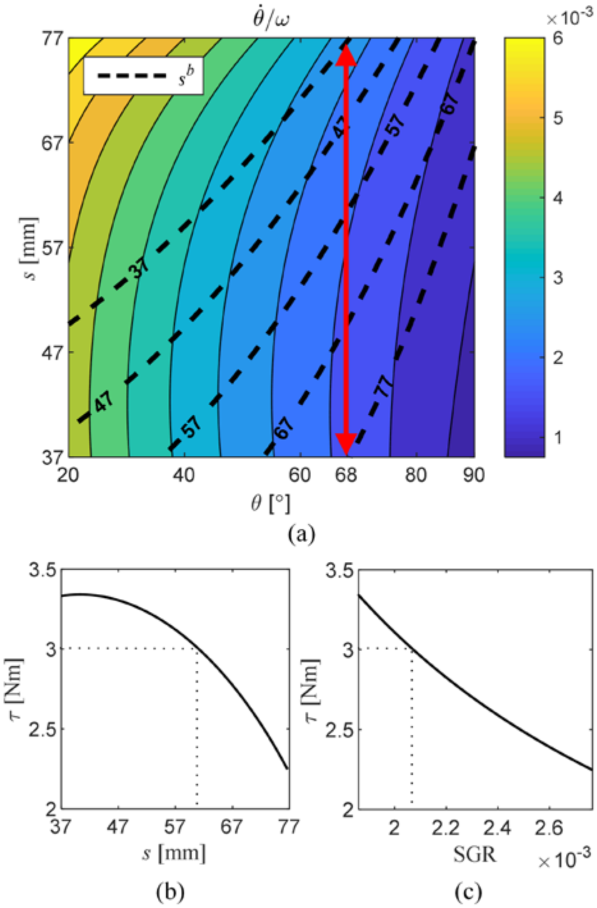

Fig. 3. Structural gear ratio (SGR) of the DAM for a single joint. (a) Contour plot of the SGR according to back slider position. (b) Plot of front slider position versus joint torque at θ = 68°. (c) Plot of the SGR versus joint torque at θ = 68°.

continuously variable gearing.

B. *Structural Gear Ratio of the DAM*

In this study, a leadscrew was used to implement the linear movement of the slider along the link. Considering the offset between a hinge joint and slider (h in Fig. 2), the relation between the joint angle (θ) and the slider positions (s) can be expressed, using the law of cosine as follows:

$$(c)^2 = (\hat{s})^2 + (\hat{s}^b)^2 - 2\hat{s}\hat{s}^b \cos(\pi - \theta)\,, \qquad (1)$$

where $\hat{s} = s - h\tan(\theta/2)$; $\hat{s}^b = s^b - h\tan(\theta/2)$;

TABLE II Specification of the motors used for the DAM and JAM

Item		DAM	JAM
Motor	Model	PGM12-1230	DCX 16 S
	ω_0 [rpm]	12500	6340
	τ_s [mNm]	3.12	12.5
	ω-τ area [W]	2.04	4.15
	Weight [g]	13	26
Gear head	Model	IG-12	GPX 16
	Ratio	1/16	1/28
Spur gear	Ratio	26/30	26/30
Harmonic drive	Model	-	CSG-17-80-2UH
	Ratio	-	1/80
SGR	Min. ratio	1/858.38	-
	Max. ratio	1/205.15	-

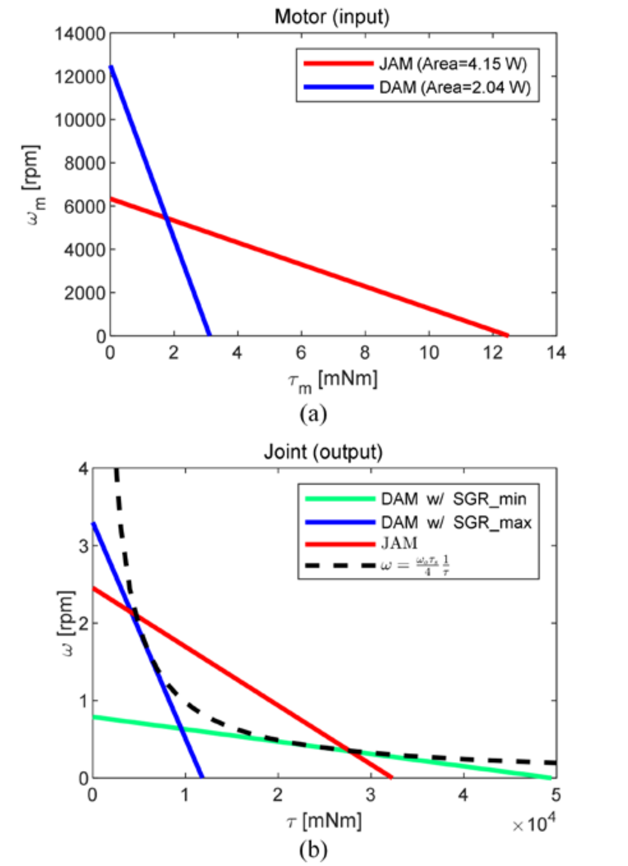

Fig. 4. Motor and joint characteristic curves. (a) Motor characteristic curves selected for the JAM and DAM. (b) Joint characteristic curves of the JAM and DAM according to the minimum and maximum SGRs.

$s^b = \sqrt{(c)^2 - (\hat{s}\sin\theta)^2} - \hat{s}\cos\theta_j + h\tan(\theta/2)$; c is the length of the connecting rod; h is the hinge offset; and s and s^b are the position of the front and back sliders, respectively. Differentiating (1) with respect to time, the angular velocity of the joint can be obtained as:

$$\dot{\theta} = \frac{\left(s - h\tan\frac{\theta}{2}\right)\left(\dot{s} + \dot{s}^b\cos\theta\right) + \left(s^b - h\tan\frac{\theta}{2}\right)\left(\dot{s}\cos\theta + \dot{s}^b\right)}{h\cos\theta(s + s^b) + \sin\theta(ss^b - h^2)}\,. \quad (2)$$

If the lead of leadscrew is L, the slider's speed $\dot{s}$ and $\dot{s}^b$ can be derived, as follows:

$$\dot{s} = \frac{L}{2\pi}\omega_j\,,\ \dot{s}^b = \frac{L}{2\pi}\omega^b\,, \qquad (3)$$

where ω and ω^b indicate the motor speed for the front and back sliders, respectively. To calculate the gear ratio, we first assume that $\omega^b = 0$, allowing us to determine the gear ratio by the front slider. In this study, the structural gear ratio (SGR) is defined, as follows:

$$SGR = \frac{\dot{\theta}}{\omega} = \frac{\cos\theta\left(s^b - h\tan\frac{\theta}{2}\right) + \left(s - h\tan\frac{\theta}{2}\right)}{h\cos\theta(s + s^b) + \sin\theta(ss^b - h^2)}\frac{L}{2\pi}\,. \qquad (4)$$

Because s^b is a function of θ and s, the SGR finally becomes a function of θ and s. In this study, using the information listed in TABLE I, the SGR was calculated to investigate the effect of the gear ratio change. Fig. 3(a) shows the contour of the SGR of the DAM for the single joint. Within a given range of

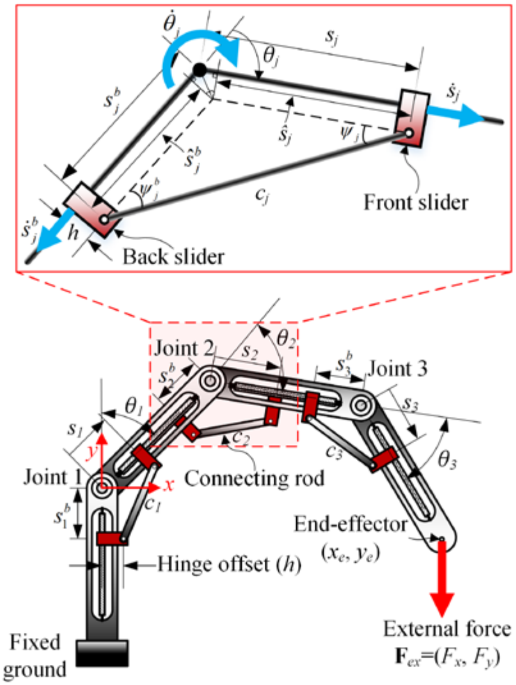

Fig. 5. Diagram of the DAM-based three-revolute joint manipulator.

the back slider position (37mm ≤ s^b ≤ 77mm), the minimum SGR is 1.16e-3 when θ = 90° and s = 66.66 mm; maximum SGR is 4.87e-3 when θ = 20° and s = 49.67 mm. Therefore, the maximum-to-minimum SGR ratio is 4.2.

To investigate a relationship between the slider position, SGR, and torque for a single joint, the torque generated at the joint can be derived [20], as follows:

$$\tau = F_{\max}\frac{s\tan\psi + h}{1+\mu\tan\psi}, \tag{5}$$

where $\psi = \cos^{-1}\left\{\left(c^2+\hat{s}^2-(\hat{s}^b)^2\right)\big/\left(2c\hat{s}\right)\right\}$; $F_{\max}$ is the maximum thrusting force of the slider; and μ is the Coulomb friction coefficient. The specific relationship between the slider position, SGR, and torque at θ = 68° is shown in Fig. 3(b) and 3(c). For example, when s is 61.02mm, the SGR becomes 2.07e-3 and this allows for the joint torque of 3Nm. The trend of the curves shown in Fig. 3(b) and 3(c) is similar

TABLE III Design Parameters of the DAM-3R

Design variables	Joint 1		Joint 2		Joint 3	
	Lower Bound	***Upper Bound***	***Lower Bound***	***Upper Bound***	***Lower Bound***	***Upper Bound***
θ_1 [°]	$\theta_1^{(l)}$	$\theta_1^{(u)}$	$\theta_2^{(l)}$	$\theta_2^{(u)}$	$\theta_3^{(l)}$	$\theta_3^{(u)}$
s_j [mm]	37.0	77.0	37.0	77.0	37.0	77.0
$\dot{s}_j$ [mm/s]	-7.1	7.1	-7.1	7.1	-7.1	7.1
$\dot{s}_j^b$ [mm/s]	-7.1	7.1	-7.1	7.1	-7.1	7.1
Design constants	**Joint 1**		**Joint 2**		**Joint 3**	
l_j [mm]	114.0		114.0		129.0	
c_j [mm]	80.0		80.0		80.0	
M			8			
$F_{\max}$ [N]			55.79			
$\dot{s}_{\max}$ [mm/s]			7.1			

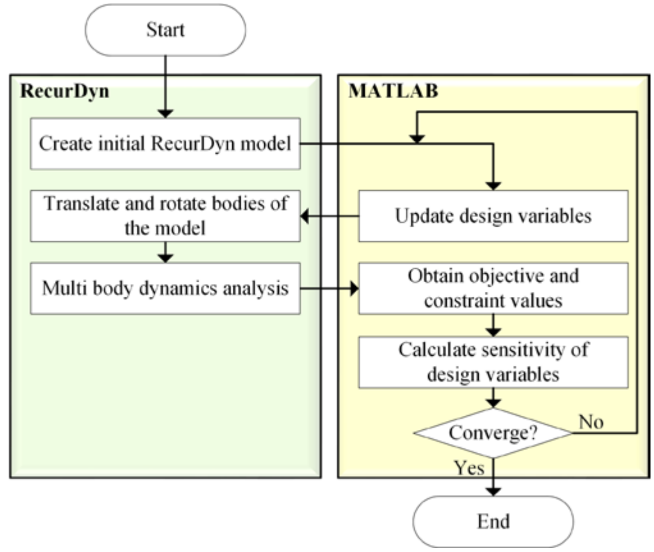

Fig. 6. Flowchart of the optimization framework.

to that reported in [11], [12]. It is interesting to note that the gear ratio in [11], [12] is passively determined according to the external load, whereas the proposed SGR can be actively controlled for a given task by changing the position of the front and back sliders, as expressed in (4). Because changing the position of the front and back sliders is a way of joint actuation in the DAM, no additional actuator is required for active gear changes in the DAM.

However, the JAM which is a widely used actuating method uses one actuator to control one joint, whereas the DAM uses two actuators, which seemingly increases the weight and complexity of a system. To fairly compare the performance of these two driving methods, commercial motors for the DAM and JAM were selected so that the ω-τ area of the DAM is half that of the JAM (i.e., power-equivalent for joint actuation), as shown in Fig. 4(a) and TABLE II. The reducer such as gear head and spur gear was selected, considering commercial products available in the market. Fig. 4(b) shows the joint characteristic curve with the minimum and maximum SGR (1.16e-3 and 4.87e-3, respectively) under the aforementioned setting. Compared with the JAM with a fixed gear ratio, the DAM can cover a wider range of speed and torque by actively changing the SGR for a given task. Assuming that the SGR can be selected from 0 to ∞ (i.e., theoretical bounds of the SGR), the DAM can cover the actuating area under the black dotted line, which can be expressed as follows:

$$\omega = \frac{\omega_0\tau_s}{4}\frac{1}{\tau}, \tag{6}$$

where ω_0 and τ_s are the no load speed and the stall torque of the motor, respectively. In summary, through using the proposed variable gearing, the DAM can produce greater velocity and force than the JAM which is equipped with a power-equivalent motor.

III. Numerical Verification

To show the effectiveness and potential of the proposed variable gearing of the DAM, a three-revolute joint planar

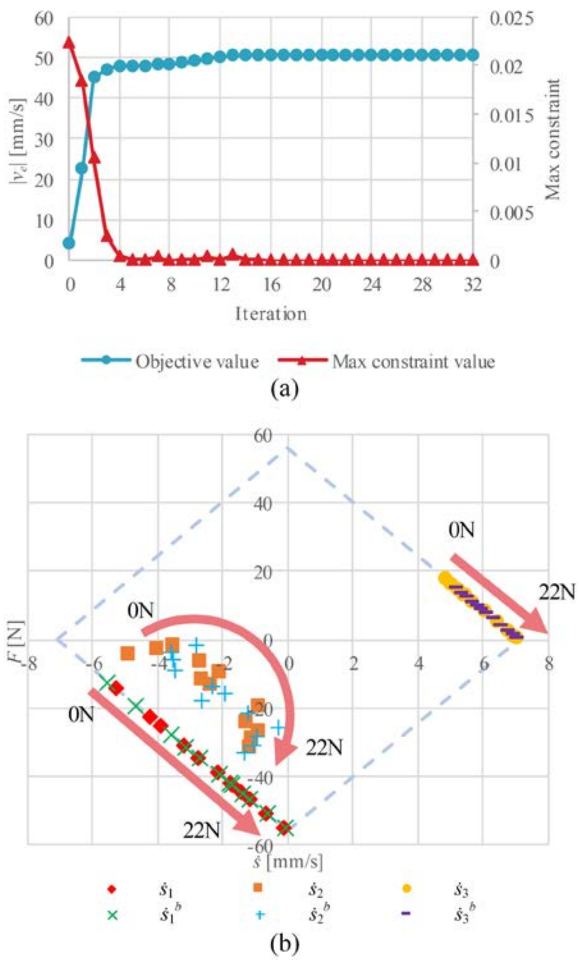

Fig. 7. Optimization results at the end-effector position (x_e, y_e) = (150 mm, -150 mm). (a) Optimization history with $\mathbf{d} = [0, 1]^T$ and $|\mathbf{F}_{ex}|$=0 where the blue and red line represent the objective function and constraint, respectively. (b) Distribution of the optimized thrusting parameters ($\dot{s}$ and F) in the linear characteristic curve of a motor with ε_k=0 to 22N.

manipulator was selected. Detailed model description and notation are shown in Fig. 5.

A. Optimization Formulation

Because the proposed variable gearing can increase either speed or force, it can be considered as a bi-objective optimization problem of maximizing velocity and force at the same time. The general bi-objective optimization formulation can be expressed as

$$\begin{array}{lll} \text{Find} & x_1, x_2, \cdots, x_n & \\ \text{To minimize} & \alpha f_1(\mathbf{x}) + (1-\alpha) f_2(\mathbf{x}) & \\ \text{subject to} & g_j(\mathbf{x}) \le 0 & j = 1, 2, \cdots, J \\ & h_k(\mathbf{x}) = 0 & k = 1, 2, \cdots, K \\ & x_i^{(L)} \le x_i \le x_i^{(L)} & i = 1, 2, \cdots, n \end{array}, \tag{7}$$

where α is a weight coefficient ($0 \le \alpha \le 1$); the superscripts (l) and (u) denote the lower and upper bounds of the design variables; f_1 and f_2 are the objective functions to be optimized simultaneously (force and speed, respectively, in this study); and g_j and h_k are the inequality and equality constraint functions, respectively. In (7), the design variable is an n-dimensional vector of **x**. One of widely used methods of solving a bi-objective optimization problem is the ε-constraint method [22]. If one objective function (velocity in this study) remains as an objective and the other (force in this study) is restricted with user-specified values as a constraint, (7) can be re-formulated as follows:

$$\begin{array}{lll} \text{Find} & x_1, x_2, \cdots, x_n & \\ \text{To minimize} & f_2(\mathbf{x}) & \\ \text{subject to} & f_1(\mathbf{x}) \le \varepsilon_m & m = 1, 2, \cdots, M \\ & g_j(\mathbf{x}) \ge 0 & j = 1, 2, \cdots, J \\ & h_k(\mathbf{x}) = 0 & k = 1, 2, \cdots, K \\ & x_i^{(L)} \le x_i \le x_i^{(L)} & i = 1, 2, \cdots, n \end{array}, \tag{8}$$

where the parameter ε_m represents an upper bound of f_1.

For the DAM, as expressed in (2), the end-effector velocity is a function of the front slider position (s) and the thrusting speed of the front and back sliders ($\dot{s}$ and $\dot{s}^b$, respectively). Finally, the detailed optimization problem can be formulated as follows:

$$\begin{array}{lll} \text{Find} & \theta_1, s_1, s_2, s_3, \dot{s}_1, \dot{s}_2, \dot{s}_3, \dot{s}_1^b, \dot{s}_2^b \ and \ \dot{s}_3^b & \\ \text{To maxmize} & f_2 = |\mathbf{v}_e| & \\ \text{Subject to} & f_1 = |\mathbf{F}_{ex}| \le \varepsilon_k & k = 1, \cdots, N \\ & g_1 = \mathbf{d}_i \cdot \mathbf{v}_e = |\mathbf{d}_i||\mathbf{v}_e| & i = 1, \cdots, M \\ & g_2 = F_j \pm \dfrac{F_{\max}}{\dot{s}_{\max}} \dot{s}_j \pm F_{\max} \le 0 & j = 1, 2, 3 \\ & g_3 = F_j^b \pm \dfrac{F_{\max}}{\dot{s}_{\max}} \dot{s}_j^b \pm F_{\max} \le 0 & j = 1, 2, 3 \\ & s_j^{(l)} \le g_4 = s_j^b \le s_j^{(u)} & j = 1, 2, 3 \\ & \theta_1^{(l)} \le \theta_1 \le \theta_1^{(u)} & \\ & s_j^{(l)} \le s_j \le s_j^{(u)} & j = 1, 2, 3 \\ & \dot{s}_j^{(l)} \le \dot{s}_j \le \dot{s}_j^{(u)} & j = 1, 2, 3 \\ & \dot{s}_j^{(l)} \le \dot{s}_j^b \le \dot{s}_j^{(u)} & j = 1, 2, 3 \end{array}. \tag{9}$$

In (9), design variables are the first joint angle (θ_1), the positions of the front slider (s_1, s_2, s_3), the thrusting speeds of the front slider ($\dot{s}_1$, $\dot{s}_2$, $\dot{s}_3$), and the thrusting speeds of the back slider ($\dot{s}_1$, $\dot{s}_2$, $\dot{s}_3$). The objective function (f_2 = $|\mathbf{v}_e|$) is the absolute value of the end-effector velocity. f_1 is a converted constraint function which represents the external force applied to the end-effector. In this study, assuming that only gravitation force is applied as external force, ε_k was set to have a range of (0, $|\mathbf{F}_{ex}|_{\max}$), where $|\mathbf{F}_{ex}|_{\max}$ represents the maximum achievable payload. g_1 is the constraint function to make the direction of end-effector velocity coincide with the base direction $\mathbf{d}_i$. In this study, the base direction $\mathbf{d}_i$ was defined, as follows:

$$\mathbf{d}_i = [\cos\beta, \sin\beta]^T, \tag{10}$$

where β is a polar angle whose range is (0, 2π). By dividing these ranges into 45 degrees, a total of eight base directions were selected (i.e., M = 8 in (9)). g_2 and g_3 are constraints indicating that the speed and force of the slider must operate within a linear characteristic curve in four quadrants. g_4 is a constraint function which represents the lower and upper bounds of the back slider position.

To solve (9), the optimization framework was constructed (Fig. 6). It is composed of the analysis module (RecurDyn) and the optimization module (in-house code written in MATLAB). RecurDyn is a commercial multi-body dynamics software, which imports a CAD model for DAM-3R and evaluate the performance such as end-effector velocity and driving force of the slider. The in-house code was built to connect the RecurDyn and optimization algorithm (Sequential quadratic programming in MATLAB optimization toolbox [23]) through exchanging information on the target system using ASCII files. The design parameters used in the optimization are summarized in TABLE III.

B. Optimization Results

Fig. 7(a) shows the optimization history at the end-effector position (x_e, y_e) = (150 mm, -150 mm) with $\mathbf{d}$=[0, 1]^T and $|\mathbf{F}_{ex}|$=0. After 13 iterations, the objective function and the maximum constraints converged to the maximum velocity (50.49 mm/s) and zero (which means that constraint becomes just feasible), respectively. The optimization results of the slider's speed and force are depicted in Fig. 7(b), where $|\mathbf{F}_{ex}|$ was applied from 0 to 22N with an increment of 2N. All the optimized points are located in the operational area (represented as the blue dotted lines in Fig. 7(b)) of a motor listed in TABLE II. It should be noted that sliders s_1, s_1^b, s_3, and s_3^b operate along the boundary of the operational area, whereas sliders s_2 and s_2^b operate inside the boundary to push the end-effector velocity to the direction of the base direction. This means that the DAM can achieve the maximum velocity without using a full power of each slider. Therefore, it is necessary to conduct optimization in order to precisely determine the optimal control parameters. Fig. 8(a) shows the Pareto frontier of end-effector velocity and force (blue line), which can be obtained as a result of (9). The sum of the mechanical power of each slider is represented as a red line. It is interesting to note that both curves in Fig. 8(a) are very similar to actual motor characteristic curves depicted in Fig. 8(b). This similarity stems from the use of the constraint functions (g_2 and g_3) which reflect the actual characteristics of the commercial motor shown in Fig. 7(b).

In addition, the JAM-3R was investigated to show the effectiveness of the proposed variable gearing. The same link length and the upper and lower bounds of joint angles were set,

TABLE IV DESIGN PARAMETERS OF THE JAM-3R

Design variables	Joint 1		Joint 2		Joint 3	
	Lower bound	*Upper bound*	*Lower bound*	*Upper bound*	*Lower bound*	*Upper bound*
θ_1 [°]	$\theta_1^{(l)}$	$\theta_1^{(u)}$	$\theta_2^{(l)}$	$\theta_2^{(u)}$	$\theta_3^{(l)}$	$\theta_3^{(u)}$
$\dot{\theta}_j$ [°/s]	-13.25	13.25	-13.25	13.25	-13.25	13.25
Design constants	Joint 1		Joint 2		Joint 3	
l_j [mm]	114.0		114.0		129.0	
M	8					
τ_{max} [Nm]	3.49					
$\dot{\theta}_{max}$ [°/s]	13.25					

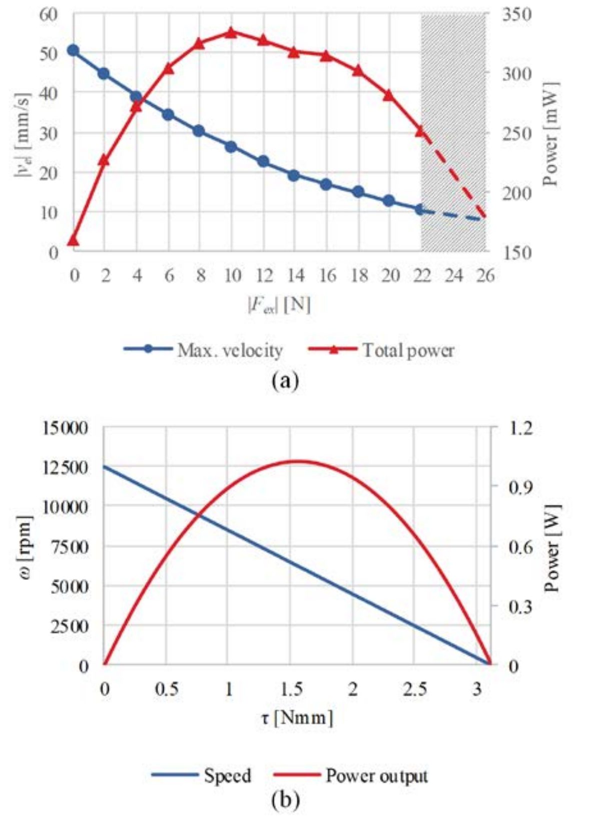

Fig. 8. (a) Pareto frontier of end-effector velocity and force (blue line) and total power (red line). Note that shaded areas are intended to show a trend of the extrapolated curves. (b) Characteristic curve of commercial motor selected for the DAM (blue line for speed and red line for power).

as used in the DAM-3R. The specification of the power-equivalent motor and reducer used for the JAM-3R were listed in TABLE II. Because end-effector velocity of the JAM-3R is determined by joint angle and angular velocity, the optimization problem for the JAM-3R is formulated as follows:

$$\begin{aligned}
&\text{Find} && \theta_1, \dot{\theta}_1, \dot{\theta}_2, \dot{\theta}_3 \\
&\text{To maxmize} && f_2 = |v_e| \\
&\text{Subject to} && f_1 = |\mathbf{F}_{ex}| = \varepsilon_k \qquad && k = 1, \cdots, N \\
& && g_1 = \mathbf{d}_i \cdot \mathbf{v}_e = |\mathbf{d}_i||\mathbf{v}_e| \qquad && i = 1, \cdots, M \\
& && g_2 = \tau_j \pm \frac{\tau_{\max}}{\dot{\theta}_{\max}} \dot{\theta}_j \pm \tau_{\max} \le 0 \qquad && j = 1,2,3 \\
& && \theta_1^{(l)} \le \theta_1 \le \theta_1^{(u)} \\
& && \dot{\theta}_j^{(l)} \le \dot{\theta}_j \le \dot{\theta}_j^{(u)} \qquad && j = 1,2,3
\end{aligned} \tag{11}$$

Design variables are the first joint angle (θ_1) and the joint speeds ($\dot{\theta}_1$, $\dot{\theta}_2$, $\dot{\theta}_3$). The objective function (f_2 = $|\mathbf{v}_e|$) represents the absolute value of the end-effector velocity, as used in (9). f_1 is a converted constraint function which represents the external force applied to the end-effector. In this study, the range of ε_k was set to have (0, $|\mathbf{F}_{ex}|_{\max}$), where $|\mathbf{F}_{ex}|_{\max}$ represents the maximum achievable payload. g_1 is the constraint function to make the direction of the end-effector velocity coincide with the base direction $\mathbf{d}_i$. g_2 is a constraint that the speed and force of the slider must operate within a

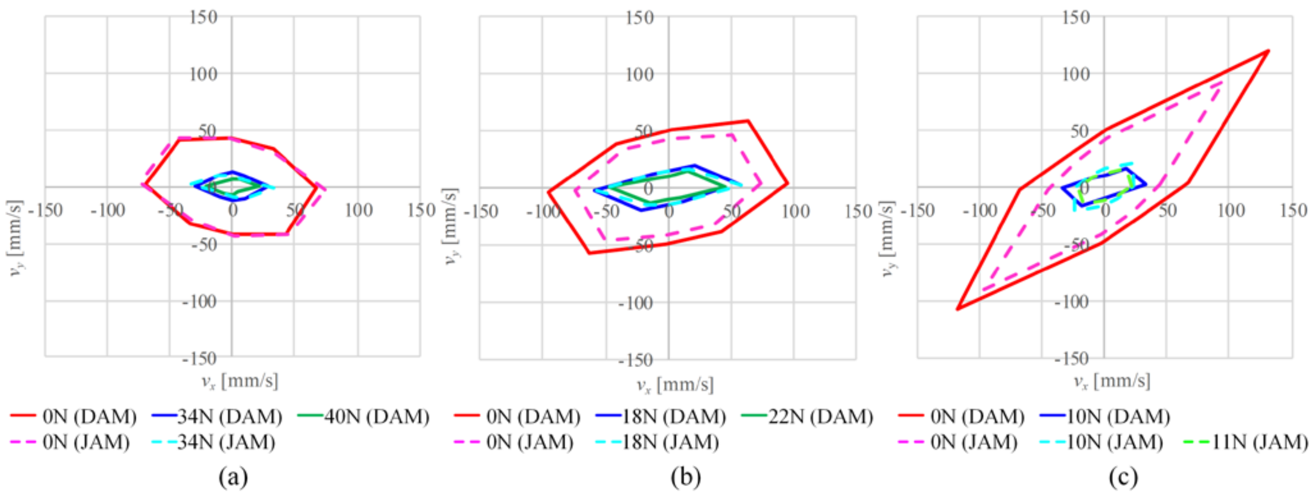

Fig. 9. Comparison of optimization results between the DAM-3R and JAM-3R at various end-effector positions. (a) $\mathbf{p}_1$ = (50 mm, -150 mm). (b) $\mathbf{p}_2$ = (150 mm, -150 mm). (c) $\mathbf{p}_3$ = (250 mm, -150 mm).

linear characteristic curve in four quadrants. The same optimization framework depicted in Fig. 6 was used to solve (11). The design parameters used in the optimization are summarized in TABLE IV.

Fig. 9 shows the maximum achievable speed according to varying payload at the end-effector positions: $\mathbf{p}_1$ = (50 mm, -150 mm), $\mathbf{p}_2$ = (150 mm, -150 mm), and $\mathbf{p}_3$ = (250 mm, -150 mm). It can be seen that the maximum achievable speed of the DAM-3R is larger than those of the JAM-3R. In addition, the DAM-3R can handle a higher payload than the JAM-3R at $\mathbf{p}_1$ and $\mathbf{p}_2$ (specifically 6N higher at $\mathbf{p}_1$ and 4N higher at $\mathbf{p}_2$), but the JAM-3R can lift 1N higher than the DAM-3R at $\mathbf{p}_3$. As the end-effector position moves from $\mathbf{p}_1$ to $\mathbf{p}_3$, the posture of the robot arm becomes extended, thereby resulting in a smaller maximum-to-minimum SGR ratio. Therefore, as the range of the SGR decreases, the motion becomes faster, but the allowable payload becomes smaller. TABLE V clearly shows that the DAM can achieve higher velocity and force than the JAM by actively changing to the optimal gear ratio for the given task.

IV. Conclusion

In this study, a novel concept of bioinspired variable gearing was proposed, based on the DAM. Through mathematical derivation, the SGR can be expressed in terms of the position of the slider and the joint angle. The optimization framework presented in this study allows to determine the optimal control parameters such as slider positions and joint angles, which can provide the maximum velocity according to the given payload. It should be noted that, because changing the position of the front and back sliders is a way of joint actuation in the DAM, the proposed bioinspired variable gearing does not require additional actuators to actively change a gear ratio. Optimization results show that the DAM can achieve higher velocity and force than the JAM by changing to the optimal gear ratio for the given task.

Because continuously variable gearing can lead to significant improvement in the performance of a robot, this research would be extended to optimize the design specification of a target robot and the optimal trajectories for a given task with further work.

TABLE V Optimization Results of Velocity and Force for the DAM-3R and JAM-3R at $\mathbf{p}_1$, $\mathbf{p}_2$, and $\mathbf{p}_3$

		DAM-3R	JAM-3R	Difference (%)
$\mathbf{p}_1$	Max $\lvert\mathbf{v}_e\rvert$ [mm/s] [a]	46.81	43.92	6.58
	Max $\lvert\mathbf{F}\rvert$ [N]	40	34	17.65
$\mathbf{p}_2$	Max $\lvert\mathbf{v}_e\rvert$ [mm/s] [a]	177.66	132.61	33.97
	Max $\lvert\mathbf{F}\rvert$ [N]	22	18	22.22
$\mathbf{p}_3$	Max $\lvert\mathbf{v}_e\rvert$ [mm/s] [a]	86.23	68.38	26.10
	Max $\lvert\mathbf{F}\rvert$ [N]	10	11	-9.09

[a] β in (10) is 45° and $\lvert\mathbf{F}_{ex}\rvert$ is 0N.

References

[1] N. Srivastava and I. Haque, “A review on belt and chain continuously variable transmissions (CVT): Dynamics and control,” *Mech. Mach. Theory*, vol. 44, no. 1, pp. 19–41, Jan. 2009.

[2] Y. J. Shin, H. J. Lee, K.-S. Kim, and S. Kim, “A Robot Finger Design Using a Dual-Mode Twisting Mechanism to Achieve High-Speed Motion and Large Grasping Force,” *IEEE Trans. Robot.*, vol. 28, no. 6, pp. 1398–1405, Dec. 2012.

[3] S. H. Jeong and K. S. Kim, “A 2-Speed Small Transmission Mechanism Based on Twisted String Actuation and a Dog Clutch,” *IEEE Robot. Autom. Lett.*, vol. 3, no. 3, pp. 1338–1345, 2018.

[4] T. Takaki and T. Omata, “High-Performance Anthropomorphic Robot Hand With Grasping-Force-Magnification Mechanism,” *IEEE/ASME Trans. Mechatronics*, vol. 16, no. 3, pp. 583–591, Jun. 2011.

[5] M. Tran, L. Gabert, M. Cempini, and T. Lenzi, “A Lightweight, Efficient Fully Powered Knee Prosthesis With Actively Variable Transmission,” *IEEE Robot. Autom. Lett.*, vol. 4, no. 2, pp. 1186–1193, Apr. 2019.

[6] N. D. Naclerio *et al.*, “Low-Cost, Continuously Variable, Strain Wave Transmission Using Gecko-Inspired Adhesives,” *IEEE Robot. Autom. Lett.*, vol. 4, no. 2, pp. 894–901, Apr. 2019.

[7] S. A. J. Spanjer, R. Balasubramanian, A. M. Dollar, and J. L. Herder, “Underactuated Gripper That Is Able to Convert from Precision to Power Grasp by a Variable Transmission Ratio,” in

Advances in Reconfigurable Mechanisms and Robots I, London: Springer London, 2012, pp. 669–679.
[8] K. Tahara, S. Iwasa, S. Naba, and M. Yamamoto, “High-backdrivable parallel-link manipulator with Continuously Variable Transmission,” in *2011 IEEE/RSJ International Conference on Intelligent Robots and Systems*, 2011, pp. 1843–1848.
[9] K. W. O’Brien *et al.*, “Elastomeric passive transmission for autonomous force-velocity adaptation applied to 3D-printed prosthetics,” *Sci. Robot.*, vol. 3, no. 23, p. eaau5543, Oct. 2018.
[10] K. V Kardong, *Vertebrates: comparative anatomy, function, evolution*, no. QL805 K35 2006. McGraw-Hill New York, 2006.
[11] E. Azizi, E. L. Brainerd, and T. J. Roberts, “Variable gearing in pennate muscles,” *Proc. Natl. Acad. Sci.*, vol. 105, no. 5, pp. 1745–1750, Feb. 2008.
[12] E. Azizi and T. J. Roberts, “Variable gearing in a biologically inspired pneumatic actuator array,” *Bioinspir. Biomim.*, vol. 8, no. 2, p. 026002, Mar. 2013.
[13] S. Itadera, E. Dean-Leon, J. Nakanishi, Y. Hasegawa, and G. Cheng, “Predictive Optimization of Assistive Force in Admittance Control-Based Physical Interaction for Robotic Gait Assistance,” *IEEE Robot. Autom. Lett.*, vol. 4, no. 4, pp. 3609–3616, 2019.
[14] K. Al Khudir, G. Halvorsen, L. Lanari, and A. De Luca, “Stable Torque Optimization for Redundant Robots Using a Short Preview,” *IEEE Robot. Autom. Lett.*, vol. 4, no. 2, pp. 2046–2053, 2019.
[15] A. Homayouni-Amlashi, A. Mohand-Ousaid, and M. Rakotondrabe, “Multi Directional Piezoelectric Plate Energy Harvesters Designed By Topology Optimization Algorithm,” *IEEE Robot. Autom. Lett.*, vol. 5, no. 2, pp. 462–469, Apr. 2020.
[16] T. Taunyazov, M. Rubagotti, and A. Shintemirov, “Constrained Orientation Control of a Spherical Parallel Manipulator via Online Convex Optimization,” *IEEE/ASME Trans. Mechatronics*, vol. 23, no. 1, pp. 252–261, Feb. 2018.
[17] C. H. Tan, D. S. Bin Shaiful, W. J. Ang, S. K. H. Win, and S. Foong, “Design Optimization of Sparse Sensing Array for Extended Aerial Robot Navigation in Deep Hazardous Tunnels,” *IEEE Robot. Autom. Lett.*, vol. 4, no. 2, pp. 862–869, Apr. 2019.
[18] T. C. Bulea, R. Kobetic, C. S. To, M. L. Audu, J. R. Schnellenberger, and R. J. Triolo, “A Variable Impedance Knee Mechanism for Controlled Stance Flexion During Pathological Gait,” *IEEE/ASME Trans. Mechatronics*, vol. 17, no. 5, pp. 822–832, Oct. 2012.
[19] A. Hassan and M. Abomoharam, “Modeling and design optimization of a robot gripper mechanism,” *Robot. Comput. Integr. Manuf.*, vol. 46, no. January, pp. 94–103, Aug. 2017.
[20] Young June Shin and Kyung-Soo Kim, “Distributed-Actuation Mechanism for a Finger-Type Manipulator: Theory and Experiments,” *IEEE Trans. Robot.*, vol. 26, no. 3, pp. 569–575, Jun. 2010.
[21] J. W. Hole, *Human anatomy & physiology*. William C Brown Communications, 1993.
[22] K. Deb, “Multi-objective Optimization,” in *Search Methodologies*, Boston, MA: Springer US, 2014, pp. 403–449.
[23] M. A. Branch and A. Grace, *Optimization Toolbox: for Use with MATLAB: User’s Guide: Version 1*. Math works, 1998.